Supplementary Material
Ultrafast electron dynamics in platinum and gold thin films driven by optical and terahertz fields

V. Unikandanunni,[1] F. Rigoni,[2] M.C. Hoffmann,[3] P. Vavassori,[4] S. Urazhdin,[5] and S. Bonetti[1, 2, a)]

[1)]*Department of Physics, Stockholm University, SE-10691 Stockholm, Sweden*

[2)]*Department of Molecular Sciences and Nanosystems, Ca' Foscari University of Venice, 30172 Venice, Italy*

[3)]*Linear Coherent Light Source, SLAC National Accelerator Laboratory, 94025 Menlo Park, CA, USA*

[4)]*CIC nanoGUNE BRTA, San Sebastian, and IKERBASQUE, Basque Foundation for Science, Bilbao, Spain*

[5)]*Department of Physics, Emory University, Atlanta, GA, USA*

I. PUMP-PROBE SETUP DETAILS

The optical laser pulses used in the experiments have a centered wavelength of 800 nm, a pulse duration of approximately 55 fs and a repetition rate of 1 kHz. We choose orthogonal polarization between the pump (s-polarized) and the probe (p-polarized) beams to eliminate the coherent artifacts which arise in the interference between energy-degenerate pulses. The pump is incident at an angle θ_{pump} = 10 degrees and the probe at an angle θ_{probe} = 45 degrees.

The intense single-cycle THz pump required for the THz pump-optical probe experiment is generated in the organic crystal DSTMS by the optical rectification of 1560 nm radiation[1], down-converted from the 800 nm fundamental using an optical parametric amplifier (OPA). The OPA is pumped with approximately 6.3 mJ pulses from the laser fundamental, and outputs 3 mJ (signal + idler). A fraction of the idler signal (0.9 mJ) is used to pump a 8 mm wide, 0.5 mm thick DSTMS crystal with approximately 1% THz conversion efficiency. This results in a few uJ of THz pulse energy, focused to a sub-mm size with a set of off-axis parabolic mirror to obtain the measured fields.

For both wavelengths, the pump is modulated with a mechanical chopper at half the laser repetition rate.

II. TWO-TEMPERATURE MODEL SIMULATIONS

We used the open-source python-based simulation package NTMpy to both solve the two-temperature model (2TM) for our material, as well as to calculate the absorbed fluence using the transfer matrix method[2]. The optical excitation was modelled with as a Gaussian-like pulse with the experimental measured with, whereas the terahertz excitation was mimicking the experimental the shape of the electric field recorded with electro-optical sampling. The physical parameters used for the 2TM simulations are reported in Table S1. All the parameters are taken from the literature except for the THz refractive index which was not available, hence we measured it using the THz time-domain spectroscopy method, as described in the next section. The electron-phonon coupling G was found overlapping the 2TM simulations with the experimental data. This is justified assuming a linear relationship between the reflectivity change and the weighted sum of the electronic and the lattice temperature change following the procedure given in Ref.[3].

[a)]Electronic mail: stefano.bonetti@fysik.su.se

TABLE S1. Table containing values of parameters used for Two-temperature model simulations

	Platinum[4–8]	Gold[4,9–14]	Silicon[15–18]
C_e(J/m^{3}K)	$740\times T_e$	$71\times T_e$	$50\times T_e$
C_l(J/m^{3}K)	2.78×10^6	2.49×10^6	2.237×10^6
k_e(W/mK)	18	315	$25\times10^{-6}T_e$
k_l(W/mK)	6.7	2.6	130
G(W/m^{3}K)[a]	$(2.5–11)\times10^{17}$	$(2.1\pm0.3)\times10^{17}$	2.8×10^{17}
ρ(kg/m^3)	21.4×10^3	19.3×10^3	2.33×10^3
n_{800}	$2.85+4.96j$	$0.15+4.91j$	$3.69+0.0066j$
n_{THz}[b]	$70+135j$	$5.3+70j$	3.42

[a] The literature value was taken as the initial guess before fine-tuning

III. THZ TIME-DOMAIN SPECTROSCOPY SAMPLE CHARACTERIZATION

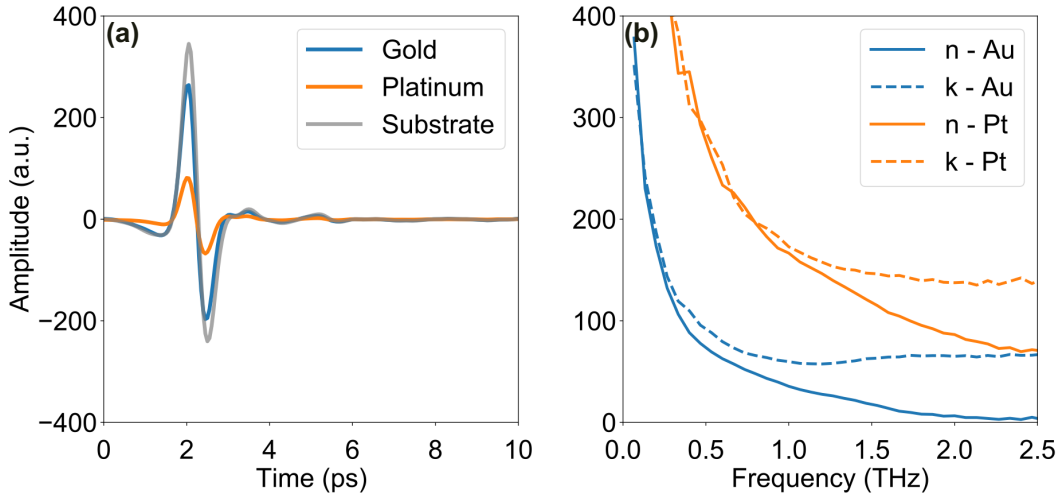

FIG. S1. (a) Terahertz time-domain transmission traces of gold and platinum thin films, and for the silicon substrate. (b) Extracted real and imaginary part of the refractive index platinum and gold.

Fig.S1(a) shows the terahertz transmission through the different samples. The relatively high THz transmission in gold indicates that the film thickness is at the percolation threshold[19,20]. The complex refractive index in Fig.S1(b) is extracted from the measured terahertz transmission using the Tinkham formula[21,22]

$$\tilde{n}^2(\omega) = 1 + i\frac{(1+n_s)c}{d\omega}\left(\frac{1}{\tilde{T}(\omega)} - 1\right), \tag{S1}$$

where $\tilde{n}(\omega)$ is the complex refractive index of the film, $\tilde{T}(\omega)$ is the complex transmittivity in frequency domain, n_s is the refractive index of the substrate, d is the thickness of the sample, and c is the speed of light. $\tilde{T}(\omega)$ is computed as the Fourier transform of the electric field transmitted by the sample on the substrate, divided it by the Fourier transform of the electric field transmitted by the bare substrate. Below ~ 0.5 THz the phase is typically not reliably measured with this technique, hence we in that region we used data linearly extrapolated from the higher frequency values, following a standard procedure[23].

IV. TRANSIENT OPTICAL REFLECTIVITY AND MATERIAL PROPERTIES

The reflectivity R for a beam impinging normally on a semi-infinite medium with refractive index $\tilde{n} = n + ik$ is

$$R = \frac{(n-1)^2 + k^2}{(n+1)^2 + k^2}, \tag{S2}$$

The relative change of reflectivity $\Delta R/R$ can be written as a function of the change in the real and imaginary parts of the dielectric constant $\tilde{\varepsilon} = \varepsilon_1 + i\varepsilon_2$, i.e.

$$\frac{\Delta R}{R} = \frac{1}{R}\left(\frac{\partial R}{\partial n}\frac{\partial n}{\partial \varepsilon_1} + \frac{\partial R}{\partial k}\frac{\partial k}{\partial \varepsilon_1}\right)\Delta\varepsilon_1 + \frac{1}{R}\left(\frac{\partial R}{\partial n}\frac{\partial n}{\partial \varepsilon_2} + \frac{\partial R}{\partial k}\frac{\partial k}{\partial \varepsilon_2}\right)\Delta\varepsilon_2, \tag{S3}$$

By evaluating the terms in the brackets, Eq. (S3) can be expanded as

$$\begin{aligned}\frac{\Delta R}{R} = &\left\{\frac{n}{n^2+k^2}\left(\frac{n-1}{(n-1)^2+k^2} - \frac{n+1}{(n+1)^2+k^2}\right) - \frac{k}{n^2+k^2}\left(\frac{k}{(n-1)^2+k^2} - \frac{k}{(n+1)^2+k^2}\right)\right\}\Delta\varepsilon_1 + \\ &\left\{\frac{k}{n^2+k^2}\left(\frac{n-1}{(n-1)^2+k^2} - \frac{n+1}{(n+1)^2+k^2}\right) + \frac{n}{n^2+k^2}\left(\frac{k}{(n-1)^2+k^2} - \frac{k}{(n+1)^2+k^2}\right)\right\}\Delta\varepsilon_2,\end{aligned} \tag{S4}$$

The coefficients of $\Delta\varepsilon_1$ and $\Delta\varepsilon_2$ are often denoted as α and β respectively and are known as Seraphin's coefficients[24]. For our gold films $\alpha \approx -0.0014$ and $\beta = -0.016$, i.e. both of them are negative with $|\alpha| < |\beta|$. This is important for the considerations later on.

In order to understand what causes the transient optical reflectivity, we need to express the variation of the complex dielectric function, i.e. $\Delta\varepsilon_1$ and $\Delta\varepsilon_2$ in terms of characteristic material parameters. We chose Drude-Lorentz model[25] with one Lorentz oscillator as a good approximation for the dielectric function of our gold films. The dielectric function $\tilde{\varepsilon}(\omega)$ is then

$$\tilde{\varepsilon}(\omega) = 1 - \frac{\omega_p^2}{\omega^2 + i\omega\gamma} + \omega_p^2 \frac{f_1}{\omega_1^2 - \omega^2 - i\omega\gamma_1}, \tag{S5}$$

where ω_p is the plasma frequency, ω_j is the resonance frequency, f_j is the oscillator strength, γ_j is the electron-electron scattering rate. The first term in Eq. (S5) is the free electron contribution to the dielectric function, whereas the second term denotes the contribution from the inter-band transition. The dielectric response at near-infrared frequencies is dominated by the free electron absorption[26]. However, inter-band transitions relatively close by the probing energy can also have a measurable effect.

The inter-band transition is from the $d-$band to the Fermi-surface and it is the dominant one close to the L point, with a resonance energy of 2.9 eV. The real and imaginary parts of the dielectric function given in Eq. (S5) are then

$$\varepsilon_1(\omega) = 1 - \frac{\omega_p^2}{\omega^2 + \gamma^2} + \omega_p^2 \frac{f_1(\omega_1^2 - \omega^2)}{(\omega_1^2 - \omega^2)^2 + \omega^2\gamma_1^2}, \tag{S6}$$

$$\varepsilon_2(\omega) = \frac{\omega_p^2\gamma}{\omega(\omega^2 + \gamma^2)} + \omega_p^2\omega \frac{f_1\gamma_1}{(\omega_1^2 - \omega^2)^2 + \omega^2\gamma_1^2}, \tag{S7}$$

The variation of the real and imaginary parts of ε at a given frequency ω can hence be due either to a change in ω_p or in γ, induced by the pump field[27]. Given that $\omega_p = \sqrt{Ne^2/\varepsilon_0 m}$, where N is the free electron density, e is the electronic charge, ε_0 is the vacuum permittivity and m is the mass of electron, a variation in the plasma frequency can be ascribed only with a variation in N. Hence we can write

$$\Delta\varepsilon_1 = A_1\Delta N/N + B_1\Delta\gamma, \tag{S8}$$

$$\Delta\varepsilon_2 = A_2\Delta N/N + B_2\Delta\gamma, \tag{S9}$$

Differentiating Eqs. (S6) and (S7) with respect to N and γ, and assuming $f_1 = c_1 N$, with c_1 a normalizing constant, gives the explicit expressions for A_1, B_1, A_2, and B_2, i.e.

$$A_1 = -\frac{\omega_p^2}{\omega^2 + \gamma^2} + 2\omega_p^2 \frac{f_1(\omega_1^2 - \omega^2)}{(\omega_1^2 - \omega^2)^2 + \omega^2\gamma_1^2}, \quad B_1 = \frac{2\omega_p^2\gamma}{(\omega^2 + \gamma^2)^2}, \tag{S10}$$

$$A_2 = \frac{\omega_p^2\gamma}{\omega(\omega^2 + \gamma^2)} + 2\omega_p^2\omega \frac{f_1\gamma_1}{(\omega_1^2 - \omega^2)^2 + \omega^2\gamma_1^2}, \quad B_2 = \frac{\omega_p^2(\omega^2 - \gamma^2)}{\omega(\omega^2 + \gamma^2)^2}, \tag{S11}$$

A. 800 nm driven dynamics

With the optical pump fields used in the experiments presented in the main text, i.e. at 1.55 eV, below the photoemission threshold, N is expected to stay constant. Hence, the change in $\tilde{\varepsilon}$ in this case must be ascribed to a variation of the scattering rate. Such variation is in turn related to the change in electronic and lattice temperatures T_e and T_l according to the expression[26]

$$\Delta\gamma = 2A_{ee}T_e\Delta T_e + B_{ep}\Delta T_l, \tag{S12}$$

where $A_{ee} = 1.7\times10^7 s^{-1}K^{-2}$ and $B_{ep} = 1.45\times10^{11}s^{-1}K^{-2}$ are the electron-electron and, respectively, the electron-phonon scattering coefficients for gold, implying $\Delta\gamma > 0$. From Eqs. (S10) and (S11), we see that $B_1, B_2 > 0$ if $\omega^2 > \gamma^2$. This is true in our case, since $\hbar\omega = 1.55$ eV and $\hbar\gamma \approx 0.1$ eV.

Thus, the variation of both the real and imaginary parts of the dielectric constant is positive, i.e. $\Delta\varepsilon_1, \Delta\varepsilon_2 > 0$. This situation, combined with the negative values of the Seraphin's coefficients α and β discussed above, leads to a negative transient reflectivity change, i.e. $\Delta R/R < 0$ for 800 nm pump-probe experiments. This is consistent with the observation in the main text. An advanced quantum mechanical treatment of the thermal modulation of the dielectric constant can be found in the work of Conforti and Della Valle[28].

B. THz driven dynamics

In the main text, we argued that the THz pump induced field emission of electrons via Fowler-Nordheim tunneling. If electrons are emitted, the free electron concentration N is reduced. A_2 in Eq. (S11) is always positive since all terms in the expressions are positive. A_1 can instead have positive or negative depending on the relative weight of the free electron term to the inter-band one. With the tabulated values for gold from Ref.[5], we obtain $\Delta R/R = (\alpha A_1 + \beta A_2)\Delta N/N \approx -6\cdot10^{-3}\Delta N/N$, which leads to a positive reflectivity change when the electron density is reduced. Adding more Lorentz-like transitions would have the effect of making the reflectivity change even more positive.

We have neglected in this last consideration the role of the electron-electron scattering rate. In the initial part of the THz-induced dynamics, $\Delta\gamma \approx 0$, since the THz energy is dissipated as kinetic energy of the emitted electrons rather than in thermalization, which occurs at later time scales. In the main text, we indeed report a small negative reflectivity change $\Delta R/R < 0$ in the later part of dynamics, which is consistent with $\Delta\gamma > 0$ and the same reasoning as for the 800 nm pump data.

V. THZ TRANSIENT REFLECTIVITY IN 50 NM FILMS

As complementary measurements, we show here the transient reflectivity driven by the THz pump on thicker (50 nm) platinum and gold films, and we compare them with the main text data in Fig. S2(a)-(b) taken on 10 nm thick films. The thicker platinum film shows a 25 times smaller reflectivity variation, and no observable signal can be measured from the thicker gold film. In Fig. S3, we compare the absorption profiles of the two materials and for the two thicknesses, using the transfer matrix method. For both materials, we observe a much lower absorption for the thicker films.

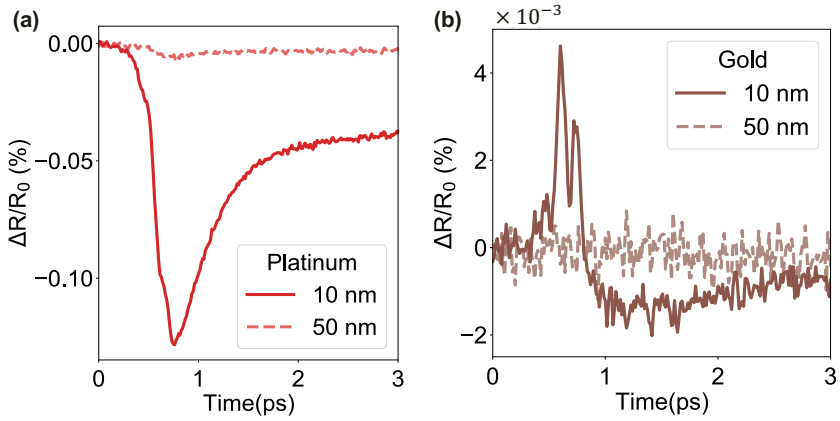

FIG. S2. Comparison of the THz-induced transient reflectivity in (a) platinum and (b) gold thin films of different thickness, all grown on a silicon substrate.

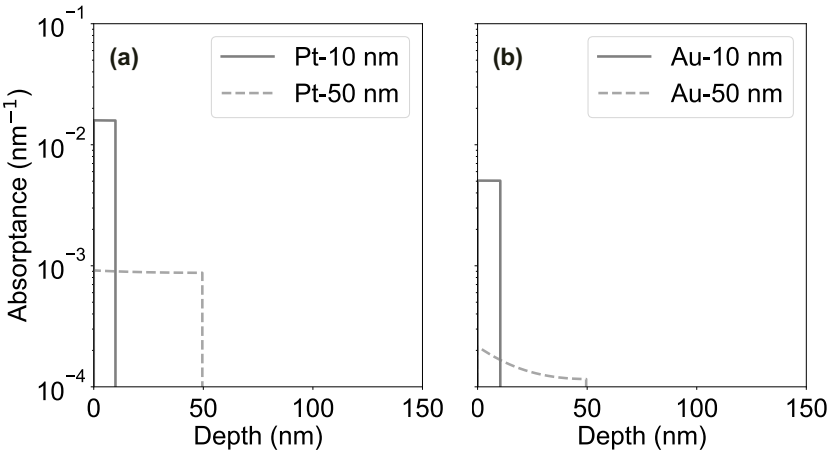

FIG. S3. THz absorption profile calculated using the transfer matrix method for (a) platinum and (b) gold films of different thickness

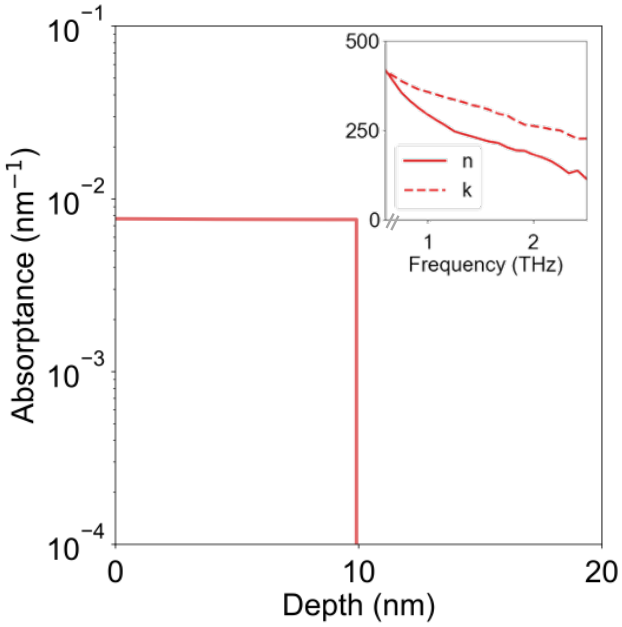

FIG. S4. THz absorption profile calculated using the transfer matrix method for sputtered gold film of thickness 10 nm. Inset: real (n) and imaginary (k) part of refractive index as a function of frequency measured using time-domain THz spectroscopy

VI. ATOMIC FORCE MICROSCOPY MEASUREMENTS

Atomic force microscopy (AFM) analysis was carried out in standard tapping mode in air (T=21.1 °C, RH=51%) using a RTESPA-300 probe (nominal tip radius: 8 nm, nominal frequency: 300 KHz, spring constant 40 N/m). AFM morphological images of the measured samples are shown in Fig. S5. Roughness analysis was carried out by Gwyddion software, and reported in Fig. S6. We have plotted the RMS roughness to thickness ratio for the three samples discussed in the main text, and for the 50 nm gold films discussed in this Supplementary Material.

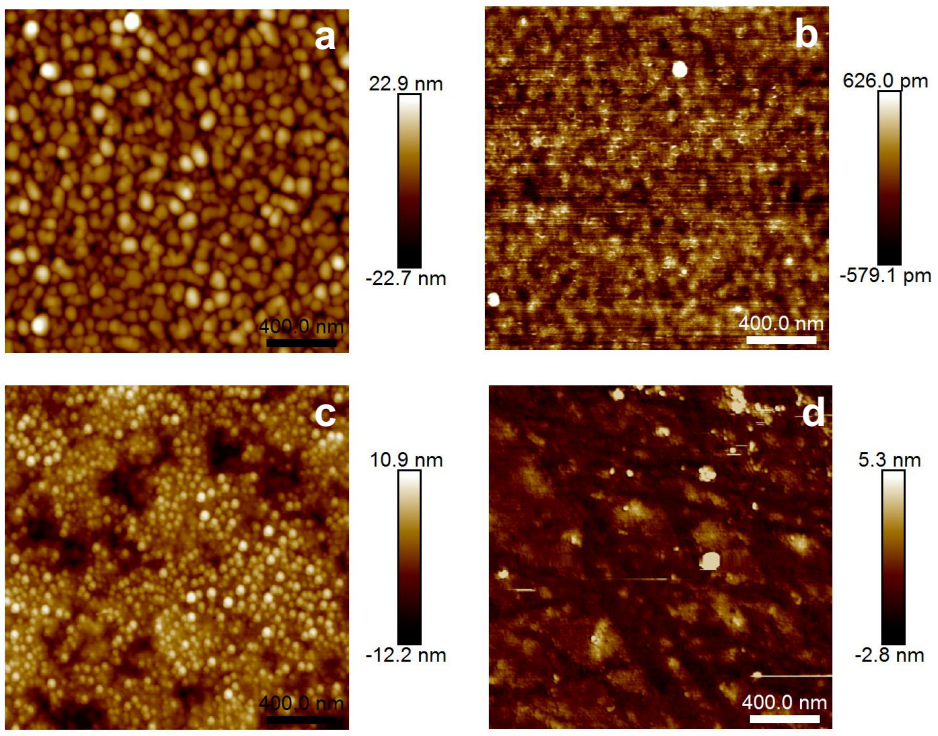

FIG. S5. AFM morphological images of the thin metallic films discussed in this work. (a) 10 nm gold on silicon substrate deposited by thermal evaporation, (b) 10 nm gold on silicon substrate deposited by sputtering, (c) 50 nm gold sample grown on silicon via thermal evaporation, (d) 10 nm platinum film on silicon substrate.

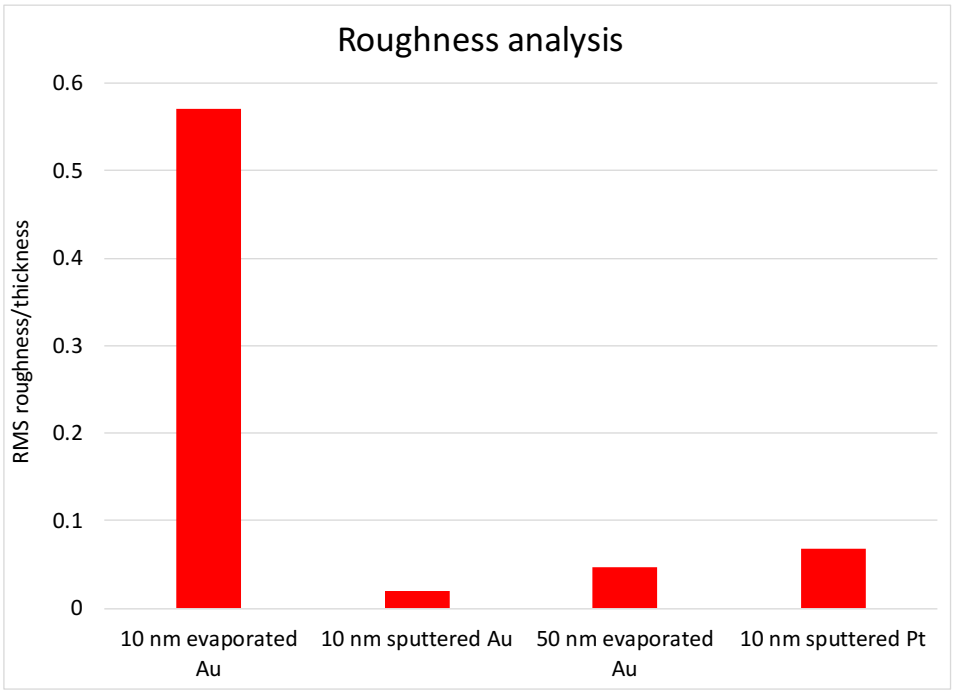

FIG. S6. Roughness analysis of measured samples.

[1] C. Vicario, A. Ovchinnikov, S. Ashitkov, M. Agranat, V. Fortov, and C. Hauri, "Generation of 0.9-mj thz pulses in dstms pumped by a cr: Mg 2 sio 4 laser," Optics letters **39**, 6632–6635 (2014).
[2] "NTMpy-N-Temperature Model solver," `https://github.com/udcm-su/NTMpy`.

[3]S. Brorson, A. Kazeroonian, J. Moodera, D. Face, T. Cheng, E. Ippen, M. Dresselhaus, and G. Dresselhaus, "Femtosecond room-temperature measurement of the electron-phonon coupling constant γ in metallic superconductors," Physical Review Letters **64**, 2172 (1990).
[4]J. Hohlfeld, S.-S. Wellershoff, J. Güdde, U. Conrad, V. Jähnke, and E. Matthias, "Electron and lattice dynamics following optical excitation of metals," Chemical Physics **251**, 237–258 (2000).
[5]A. D. Rakić, A. B. Djurišić, J. M. Elazar, and M. L. Majewski, "Optical properties of metallic films for vertical-cavity optoelectronic devices," Applied optics **37**, 5271–5283 (1998).
[6]D. E. Gray, "American institute of physics handbook," AmJPh **32**, 389–389 (1964).
[7]Y. Wang, Z. Lu, and X. Ruan, "First principles calculation of lattice thermal conductivity of metals considering phonon-phonon and phonon-electron scattering," Journal of applied Physics **119**, 225109 (2016).
[8]M. Duggin, "The thermal conductivities of aluminium and platinum," Journal of Physics D: Applied Physics **3**, L21 (1970).
[9]N. Smirnov, "Copper, gold, and platinum under femtosecond irradiation: Results of first-principles calculations," Physical Review B **101**, 094103 (2020).
[10]D. I. Yakubovsky, Y. V. Stebunov, R. V. Kirtaev, G. A. Ermolaev, M. S. Mironov, S. M. Novikov, A. V. Arsenin, and V. S. Volkov, "Au-mos2 interfaces: Ultrathin and ultrasmooth gold films on monolayer mos2 (adv. mater. interfaces 13/2019)," Advanced Materials Interfaces **6**, 1970082 (2019).
[11]A. Block, M. Liebel, R. Yu, M. Spector, Y. Sivan, F. G. de Abajo, and N. F. van Hulst, "Tracking ultrafast hot-electron diffusion in space and time by ultrafast thermomodulation microscopy," Science advances **5**, eaav8965 (2019).
[12]E. D. Palik, *Handbook of optical constants of solids*, Vol. 3 (Academic press, 1998).
[13]A. P. Caffrey, P. E. Hopkins, J. M. Klopf, and P. M. Norris, "Thin film non-noble transition metal thermophysical properties," Microscale Thermophysical Engineering **9**, 365–377 (2005).
[14]P. B. Johnson and R.-W. Christy, "Optical constants of the noble metals," Physical review B **6**, 4370 (1972).
[15]Z. Kan, Q. Zhu, H. Ren, and M. Shen, "Femtosecond laser-induced thermal transport in silicon with liquid cooling bath," Materials **12**, 2043 (2019).
[16]D. E. Aspnes and A. Studna, "Dielectric functions and optical parameters of si, ge, gap, gaas, gasb, inp, inas, and insb from 1.5 to 6.0 ev," Physical review B **27**, 985 (1983).
[17]J. Dai, J. Zhang, W. Zhang, and D. Grischkowsky, "Terahertz time-domain spectroscopy characterization of the far-infrared absorption and index of refraction of high-resistivity, float-zone silicon," JOSA B **21**, 1379–1386 (2004).
[18]J. Thorstensen and S. Erik Foss, "Temperature dependent ablation threshold in silicon using ultrashort laser pulses," Journal of Applied Physics **112**, 103514 (2012).
[19]K. Yoshioka, Y. Minami, K.-i. Shudo, T. D. Dao, T. Nagao, M. Kitajima, J. Takeda, and I. Katayama, "Terahertz-field-induced nonlinear electron delocalization in au nanostructures," Nano letters **15**, 1036–1040 (2015).
[20]M. Walther, D. Cooke, C. Sherstan, M. Hajar, M. Freeman, and F. Hegmann, "Terahertz conductivity of thin gold films at the metal-insulator percolation transition," Physical Review B **76**, 125408 (2007).
[21]R. Glover III and M. Tinkham, "Conductivity of superconducting films for photon energies between 0.3 and 4 0 k t c," Physical Review **108**, 243 (1957).
[22]A. Paulke, *Transient Conductivity Measurements using Terahertz Time-Domain Spectroscopy*, Ph.D. thesis, PhD thesis, UNIVERSITAT POTSDAM (2013).
[23]L. Duvillaret, F. Garet, and J.-L. Coutaz, "A reliable method for extraction of material parameters in terahertz time-domain spectroscopy," IEEE Journal of selected topics in quantum electronics **2**, 739–746 (1996).
[24]B. Seraphin and N. Bottka, "Band-structure analysis from electro-reflectance studies," Physical Review **145**, 628 (1966).
[25]J. D. Jackson, "Classical electrodynamics," (1999).
[26]A. N. Smith and P. M. Norris, "Influence of intraband transitions on the electron thermoreflectance response of metals," Applied Physics Letters **78**, 1240–1242 (2001).
[27]R. Rosei and D. W. Lynch, "Thermomodulation spectra of al, au, and cu," Physical Review B **5**, 3883 (1972).
[28]M. Conforti and G. Della Valle, "Derivation of third-order nonlinear susceptibility of thin metal films as a delayed optical response," Physical Review B **85**, 245423 (2012).